Solid-solution reaction suppresses the Jahn-Teller effect of potassium manganese hexacyanoferrate for potassium-ion batteries

Bingqiu Liu[a], Qi Zhang[a], Usman Ali[a], Yiqian Li[a], Yuehan Hao[a], Lingyu Zhang[a], Zhongmin Su[a], Lu Li*[a] and Chungang Wang*[a]

[a]Faculty of Chemistry, Northeast Normal University, Changchun, 130024, P. R. China.

*E-mail: lil106@nenu.edu.cn, wangcg925@nenu.edu.cn

Materials

Poly (acrylic acid) (PAA, M_W ≈ 1800) was purchased from Sigma-Aldrich (USA). Potassium carbonate (K_2CO_3), manganous chloride tetrahydrate ($MnCl_2{\cdot}4H_2O$, 99.0%), $K_4Fe(CN)_6{\cdot}3H_2O$, $MnSO_4$, aqueous ammonia solution, anhydrous ethanol, and isopropyl alcohol were obtained from Sinopharm Chemical Reagent Beijing Co., Ltd and used without further purification. Hydrochloric acid and hydrofluoric acid were obtained from Beijing Chemical Industry Group Co., Ltd. Deionized water was used in all experiments.

Synthesis of KMnHCF-S

In a 1 L flask, a PAA aqueous solution (0.2 g mL^{-1}, 2 mL) and 360 mg K_2CO_3 were added in deionized water (200 mL) and ultrasonically dispersed for 30 min. After that, IPA (800 mL) was dripped into the flask under magnetic stirring to form a suspension. Subsequently, 680 mg $MnCl_2{\cdot}4H_2O$ was added into the suspension under magnetic stirring for 1 h to obtain the $Mn(OH)_2$/PAA-K NSs. The obtained $Mn(OH)_2$/PAA-K NSs were centrifuged and washed with deionized water once and then dispersed in 60 mL anhydrous ethanol for further experiment. 640 mg $K_4Fe(CN)_6{\cdot}3H_2O$ was dispersed in 320 mL deionized water and 320 mL anhydrous ethanol. The latter solution was slowly poured into the former under magnetic stirring. After 12 h, the resulting precipitates were centrifuged, washed several times with deionized water, and dried under vacuum at 110 ˚C for 24 h.

Synthesis of KMnHCF-M

In a 1 L flask, PAA aqueous solution (0.2 g mL^{-1}, 2 mL) and $NH_3 \cdot H_2O$ (2 mol L^{-1}, 3 mL) were added in deionized water (200 mL) and ultrasonically dispersed for 30 min. After that, IPA (800 mL) was dripped into the flask under magnetic stirring to form a suspension. Subsequently, 680 mg $MnCl_2 \cdot 4H_2O$ was added into the suspension under magnetic stirring for 1 h to obtain the $Mn(OH)_2$/PAA-NH_4 NSs. The obtained $Mn(OH)_2$/PAA-NH_4 NSs were centrifuged and washed with deionized water once and then dispersed in 60 mL anhydrous ethanol for further experiment. 640 mg $K_4Fe(CN)_6 \cdot 3H_2O$ was dispersed in 320 mL deionized water and 320 mL anhydrous ethanol. The latter solution was slowly poured into the former under magnetic stirring. After 12 h, the resulting precipitates were centrifuged, washed several times with deionized water, and dried under vacuum at 110 ˚C for 24 h.

Synthesis of KMnHCF-L

Typically, 844 mg $K_4Fe(CN)_6 \cdot 3H_2O$ and 302 mg $MnSO_4$ were dissolved in 100 mL, and 100 mL saturated KCl solution, respectively. Then, the latter solution was slowly dropped into the former with magnetic stirring at 60 °C. After 12 h, the formed precipitate was centrifuged and washed with deionized water and anhydrous ethanol. Finally, the product was obtained after drying under a vacuum at 110 ˚C for 24 h.

Characterization

Transmission electron micrographs (TEM) were taken by JEOLJEM-2100F transmission electron microscope under a 200 kV accelerating voltage. High-resolution TEM (HRTEM) characterizations were recorded by a TECNAI G2 F20 transmission electron microscope under 200 kV accelerating voltage. Scanning electron microscopy (SEM) images were obtained by using an XL30 ESEM-FEG field-emission scanning electron microscope (FEI Co.). X-ray diffraction (XRD) patterns were obtained on a Rigaku D/max-IIB X-ray diffractometer with Cu Kα radiation. XPS was performed with an ECSALAB 250 by using non-monochromated Al Kα radiation. Raman spectra were recorded at room temperature with a JY HR-800 LabRam confocal Raman microscope in a backscattering configuration with an excitation

wavelength of 325 nm. TG analysis was carried out on a Perkin-Elmer TG-7 analyzer heated from room temperature to 300 °C at a ramp rate of 10 °C min^{-1} in air.

Electrochemical Tests

The electrochemical performance of the samples were evaluated in K test cells. The working electrodes were fabricated by mixing active materials, acetylene black, and polyvinylidene fluoride (PVDF) binder at a weight ratio of 7:2:1 in N-methylpyrrolidone (NMP) to form a high dispersed slurry. The slurry was then coated on an Al foil and dried at 90 °C for 12 h in vacuo. The KIBs were assembled in an argon-filled glove box. Potassium metal was used as the counter electrode. The electrolyte was 1 M KPF_6 dissolved in a 1:1:1 mixture of ethylene carbonate (EC), diethyl carbonate (DEC), and propylene carbonate (PC). The discharge-charge cycling was performed within a voltage range of 2.0-4.5 V on a battery test instrument (CT2001A, LAND, China) at ambient temperature. CV was implemented on a CHI760E electrochemical workstation between 2.0-4.5 V. AC electrochemical impedance spectra (EIS) were obtained on a CHI760E electrochemical workstation in the frequency range of 100 kHz to 0.01 Hz. Linear sweep voltammetry (LSV) was conducted with stainless steel serving as the working electrode and potassium metal as both counter and reference electrodes. The LSV measurements were carried out on a CHI760E with a scan rate of 0.2 mV s^{-1} from 3 to 6 V vs. K/K^+. In the case of K-ion full cells, graphite was chosen as the active material for the anode. The graphite electrode was prepared by mixing 80 wt% graphite, 10 wt% acetylene black, and 10 wt% PVDF dissolved in NMP to form a slurry. The mixture was spread on an Al foil, which was used as an anode after drying. The anode electrode was precycled for five cycles in half-cells and then assembled into full cells. In this study, the weight ratio of the cathode material (KMnHCF-S)/anode material (graphite) was about 1:2.

Calculation Methodes

All the calculations were carried out by means of spin-polarized density functional theory (DFT) methods using Vienna Ab-initio Simulation Package (VASP).[1-3] The exchange and correlation energies were described by the generalized gradient approximation (GGA) with the Perdew-Burke-Ernzerhof (PBE) functional.[4, 5] The

projector augmented-wave (PAW) method was used to describe the electron-ion interactions.[6, 7] Based on our careful convergence tests, the plane wave energy cutoff was set to 520 eV. The convergence criterion of the electronic structure was set to 10^{-6} eV, and the atomic relaxation was continued until the forces acting on atoms were smaller than 0.01 eV/Å. The Brillouin zone was sampled with 5×5×3 Monkhorst-Pack k-point mesh for the tetragonal phase and 3×3×3 for others. Gaussian smearing of 0.05 eV is applied to speed up electronic convergence.

The final structure was illustrated with VESTA software.[8]

The reaction energy for the $K_2MnFe(CN)_6$ system was calculated through:

$$E = -\left[\frac{E\left(K_{X2}MnFe(CN)_6\right) - E\left(K_{X1}MnFe(CN)_6\right)}{\Delta x} - E(K)\right]$$

where E is the reaction energy. $E(K_XMnFe(CN)_6)$ and E(K) represent the DFT calculated energies of $K_XMnFe(CN)_6$ and K.[9]

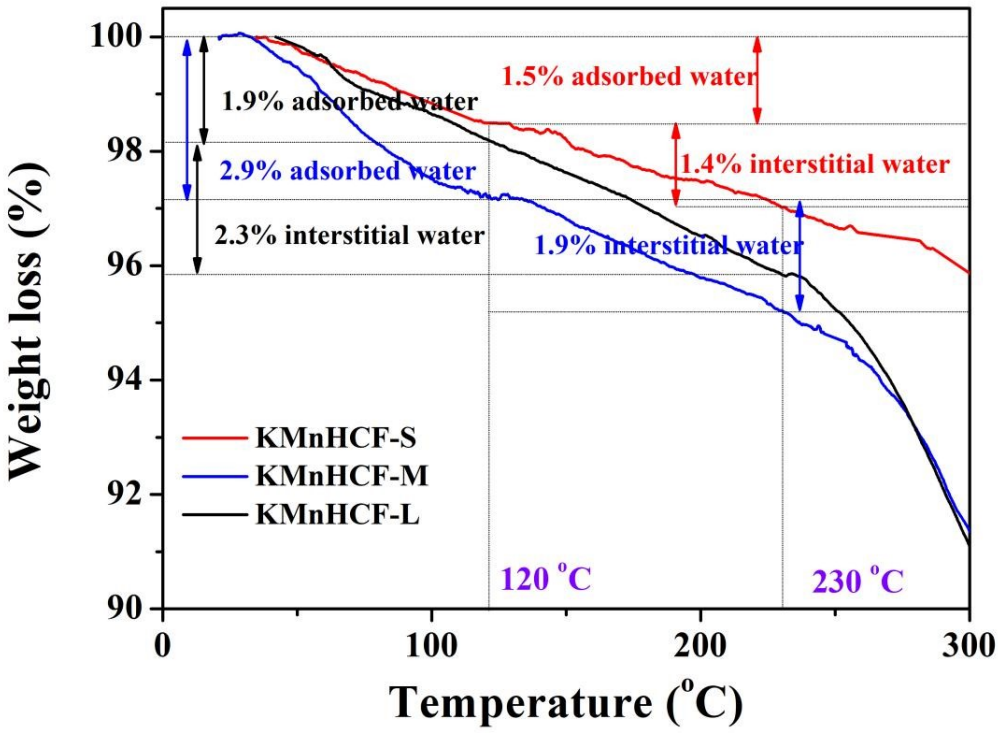

Fig. S1 TG curves of the three samples.

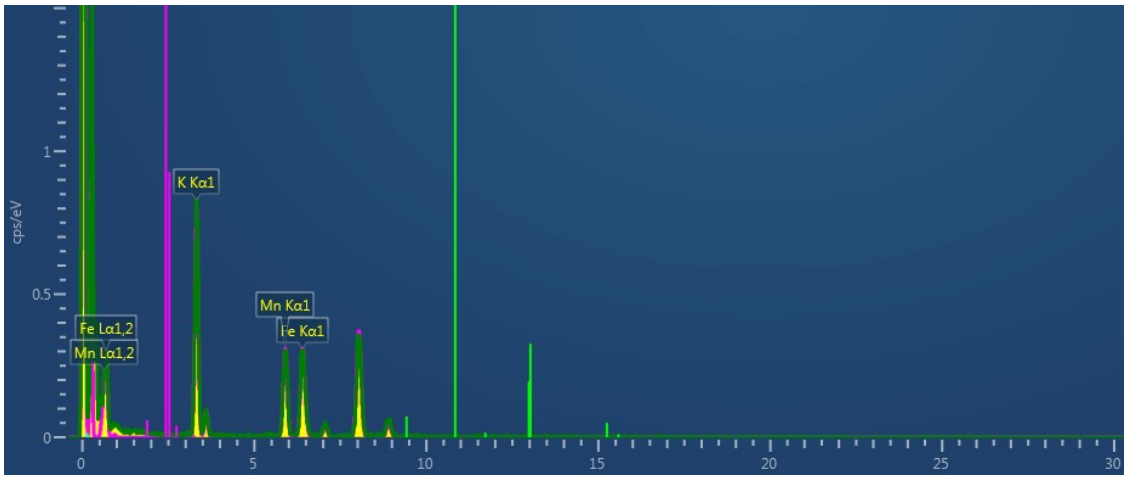

Fig. S2 Energy dispersive X-ray (EDX) spectrum of KMnHCF-S by HRTEM.

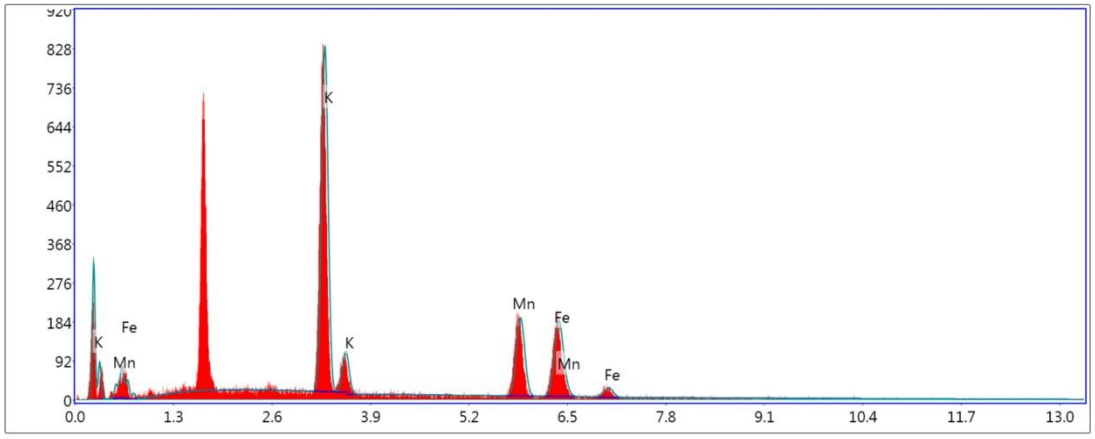

Fig. S3 Energy dispersive X-ray (EDX)spectra of KMnHCF-S by SEM.

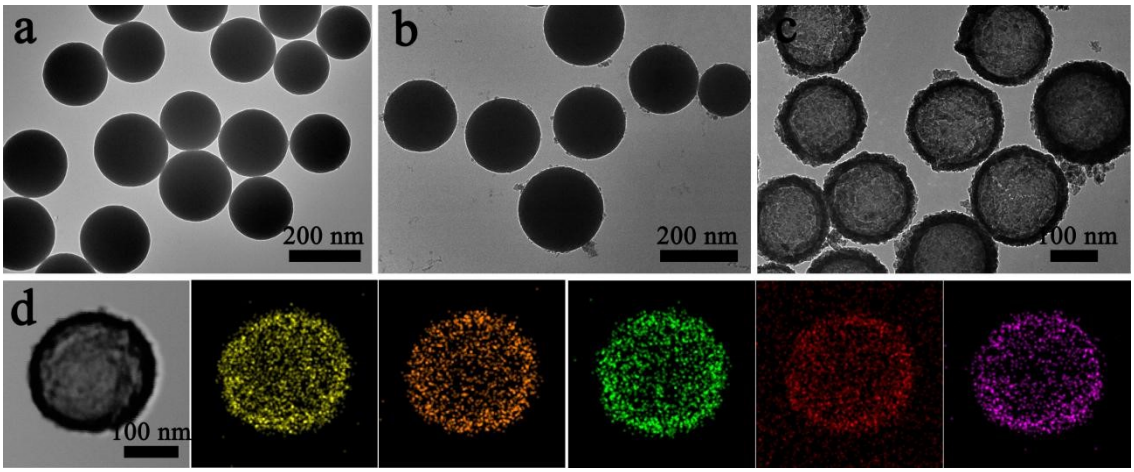

Fig. S4 HRTEM images of (a) PAA-NH_4 NSs, (b) PAA-NH_4/$Mn(OH)_2$ NSs, (c) KMnHCF-M. The elemental mapping images of a single KMnHCF-M NS: (j) TEM image and corresponding element K, Mn, Fe, C, N.

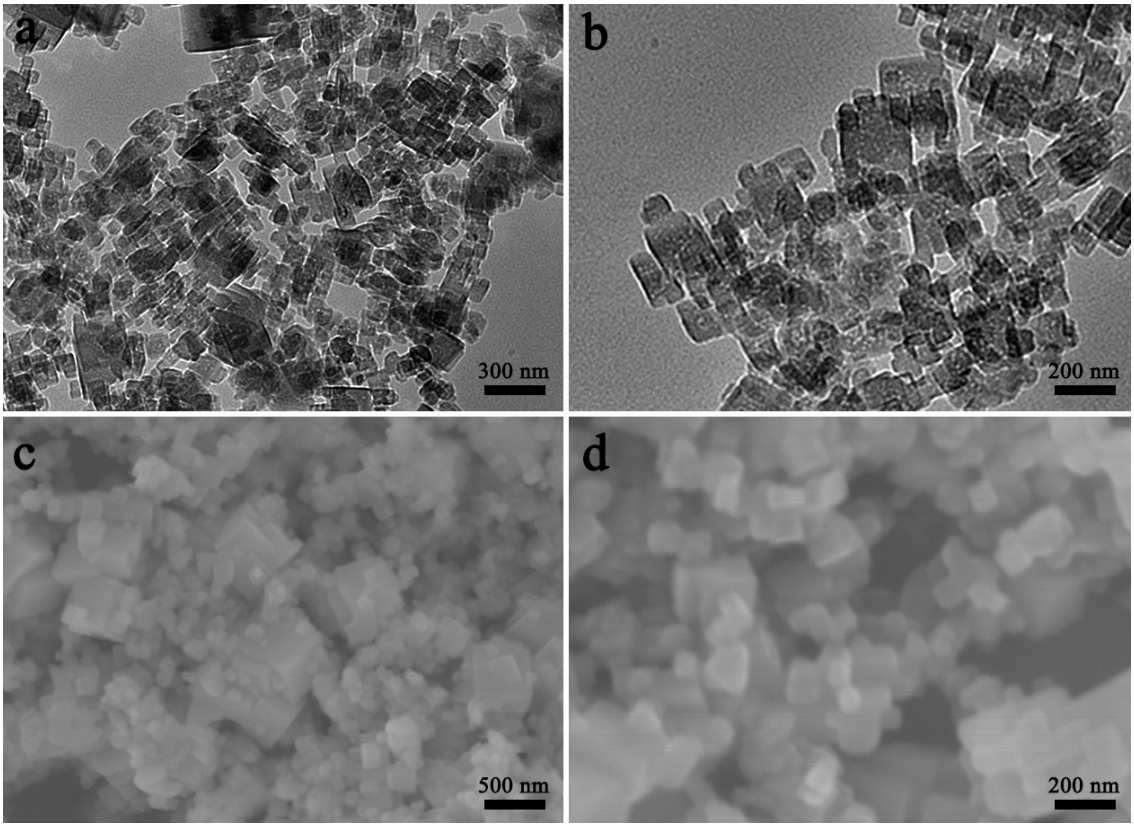

Fig. S5 (a), (b) HRTEM images of KMnHCF-L. (c), (d) SEM images of KMnHCF-L.

Table S1. ICP results of KMnHCF-S.

$K_{1.98}Mn[Fe(CN)_6]_{0.98}\cdot 0.27H_2O$			
Element	K	Mn	Fe
mole ratio	1.98	1	0.98

Table S2. ICP results of KMnHCF-M.

$K_{1.92}Mn[Fe(CN)_6]_{0.95}\cdot 0.36H_2O$			
Element	K	Mn	Fe
mole ratio	1.92	1	0.95

Table S3. ICP results of KMnHCF-L.

$K_{1.96}Mn[Fe(CN)_6]_{0.94}\cdot 0.43H_2O$			
Element	K	Mn	Fe
mole ratio	1.96	1	0.94

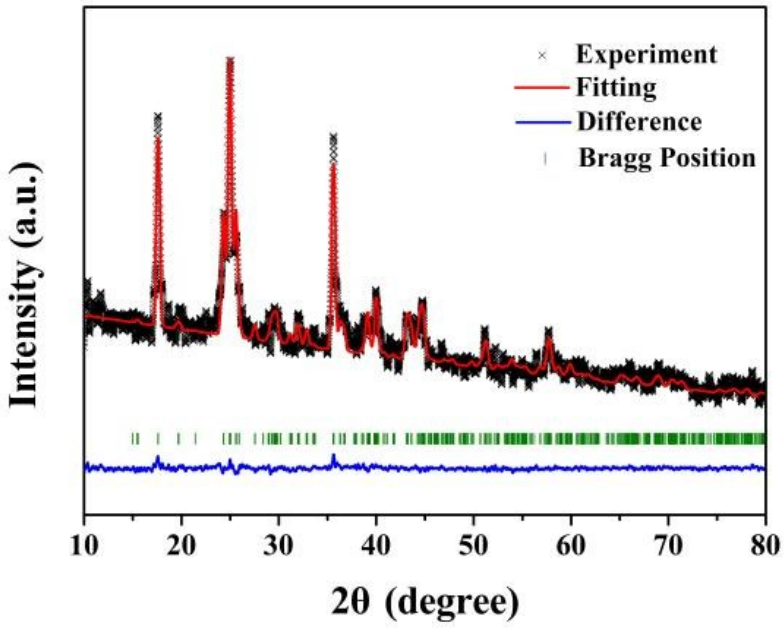

Fig. S6 Refined XRD pattern of KMnHCF-M.

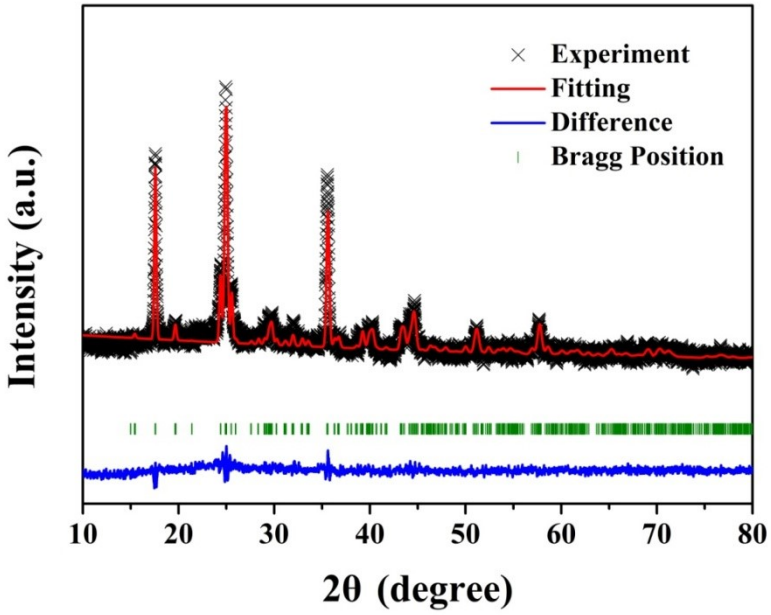

Fig. S7 Refined XRD pattern of KMnHCF-L.

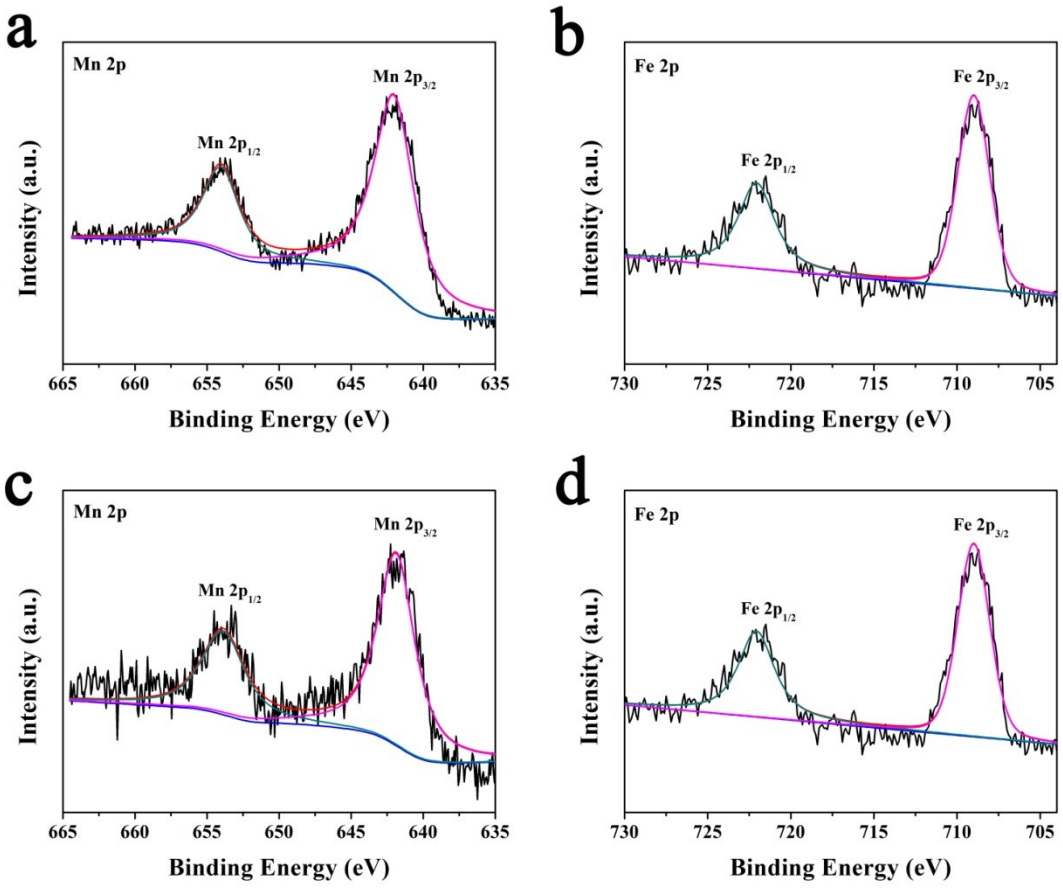

Fig. S8 (a) Mn 2p and (b) Fe 2p fitting spectra of KMnHCF-M. (c) Mn 2p and (d) Fe 2p fitting spectra of KMnHCF-L.

Table S4. Structural parameters of KMnHCF-S from Rietveld analysis.

Atom	Wyckoff	x	y	z	Occupancy
Mn	2a	0	0.5	0.5	1
Fe	2a	0	0	0	1
N	4e	0.47021	0.25227	0.83430	1
N	4e	0.03710	0.35614	0.73414	1
N	4e	0.20024	0.47524	0.39726	1
C	4e	0.55563	0.65368	0.25484	1
C	4e	0.95946	0.77858	0.15362	1
C	4e	0.69629	0.51524	0.54933	1
K	4e	0.75297	0.93865	0.48024	0.96
S.G. p21/n	a=10.091, b=7.333, c=6.975 Å, α=γ= 90^{o} β= 90.07 ^{o}				
Rp=5.41%, Rwp=8.83%, Chi2=0.81					

Table S5. Structural parameters of KMnHCF-M from Rietveld analysis.

Atom	Wyckoff	x	y	z	Occupancy
Mn	2a	0	0.5	0.5	1
Fe	2a	0	0	0	1
N	4e	0.46319	0.26825	0.83024	1
N	4e	0.04381	0.33859	0.74871	1
N	4e	0.19721	0.47545	0.39611	1
C	4e	0.55129	0.63233	0.27642	1

C	4e	0.96108	0.78613	0.14314	1
C	4e	0.69186	0.50803	0.56089	1
K	4e	0.74613	0.93917	0.48104	0.93
S.G. p21/n	a=10.126, b=7.346, c=6.965 Å, α=γ= 90^{o} β= 90.07 ^{o}				
Rp=3.91%, Rwp=6.38%, Chi2=0.46					

Table S6. Structural parameters of KMnHCF-L from Rietveld analysis.

Atom	Wyckoff	x	y	z	Occupancy
Mn	2a	0	0.5	0.5	1
Fe	2a	0	0	0	1
N	4e	0.46564	0.26106	0.83817	1
N	4e	0.04264	0.34585	0.75035	1
N	4e	0.20198	0.47465	0.39916	1
C	4e	0.56515	0.65209	0.25924	1
C	4e	0.97189	0.77931	0.15625	1
C	4e	0.69385	0.51634	0.55754	1
K	4e	0.74352	0.94441	0.48302	0.94
S.G. p21/n	a=10.112, b=7.311, c=6.984 Å, α=γ= 90^{o} β= 90.06 ^{o}				
Rp=4.03%, Rwp=7.12%, Chi2=0.62					

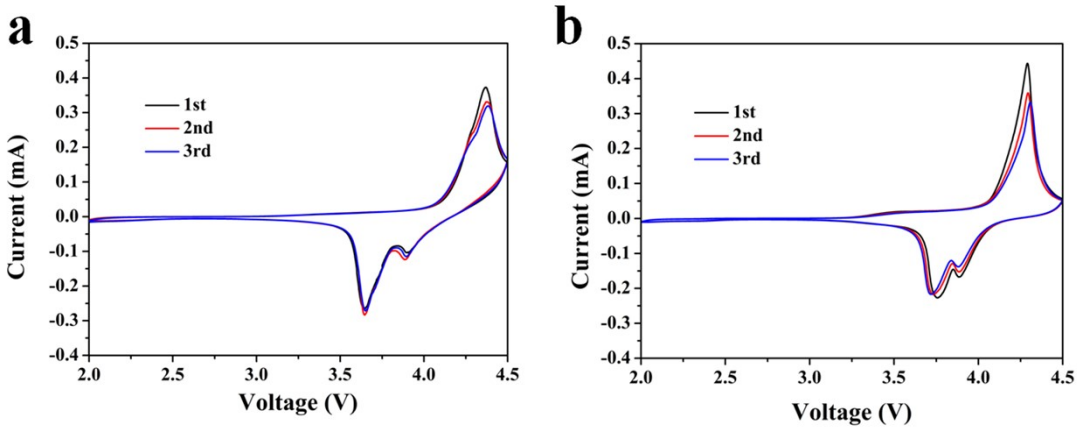

Fig. S9 CV curves of (a) KMnHCF-M and (b) KMnHCF-L at 0.1 mV s^{-1}.

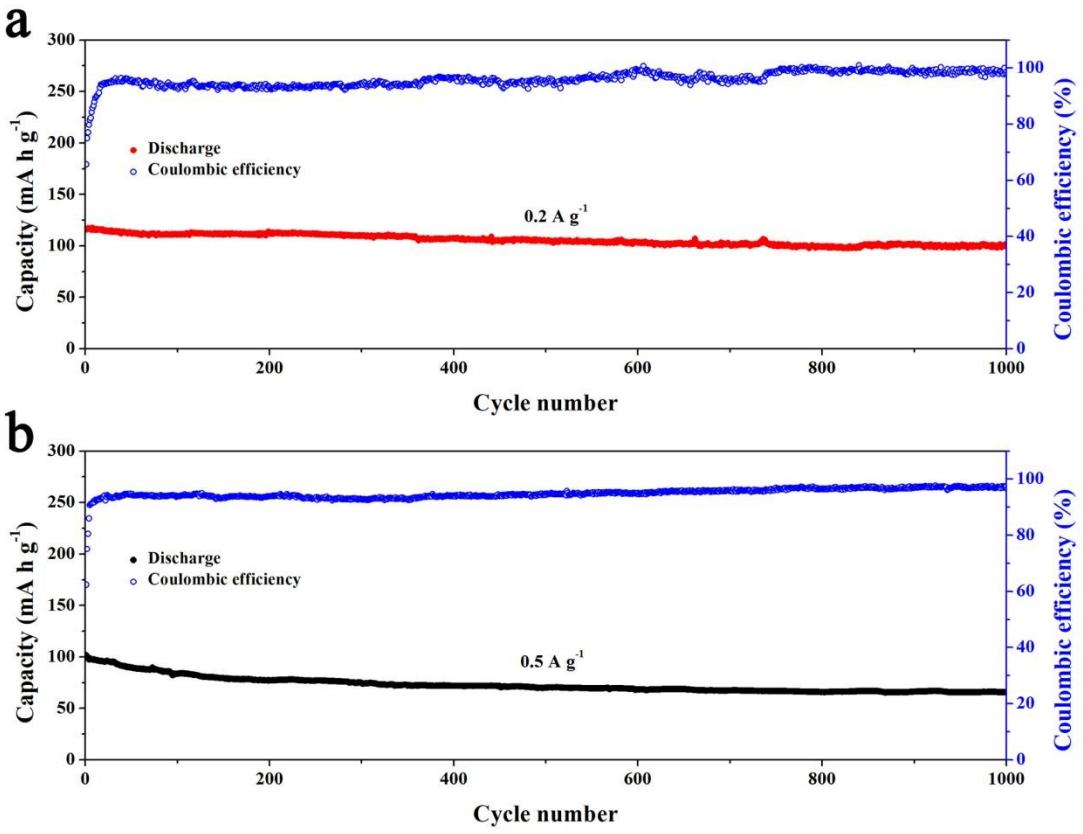

Fig. S10 Cycling performance of KMnHCF-S at (a) 0.2 A g^{-1} and (b) 0.5 A g^{-1} for 1000 cycles.

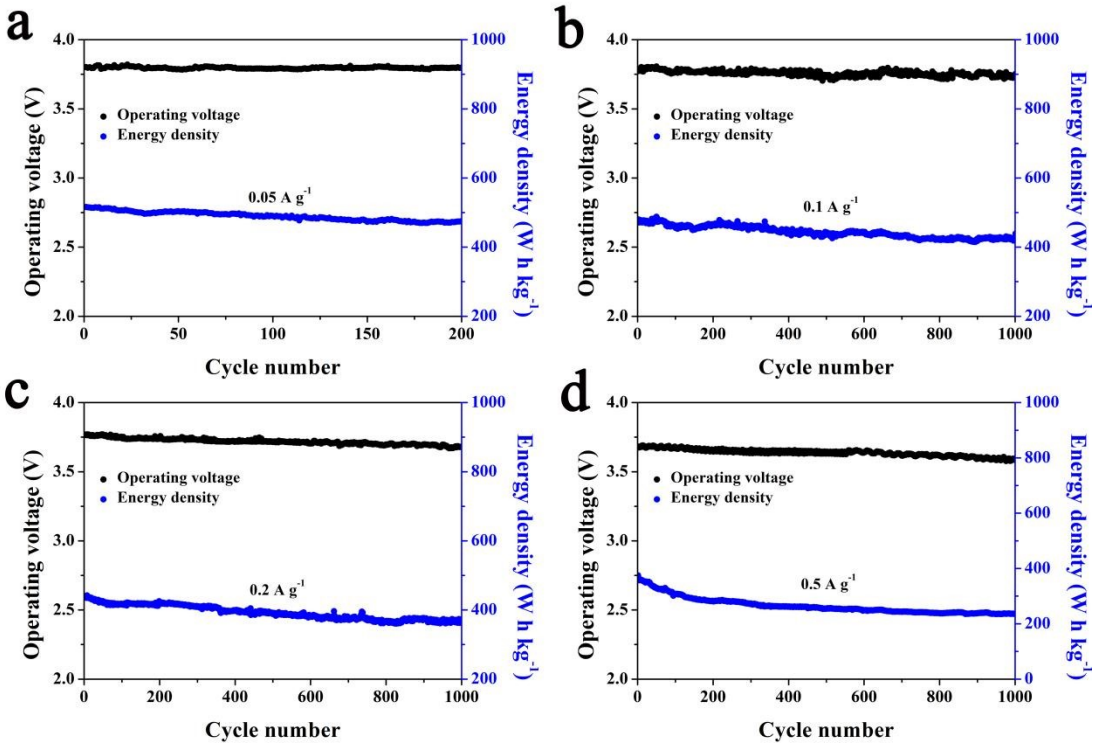

Fig. S11 Operating voltage and energy density of KMnHCF-S at (a) 0.05 A g^{-1}, (b) 0.1 A g^{-1} (c) 0.2 A g^{-1} and (d) 0.5 A g^{-1}.

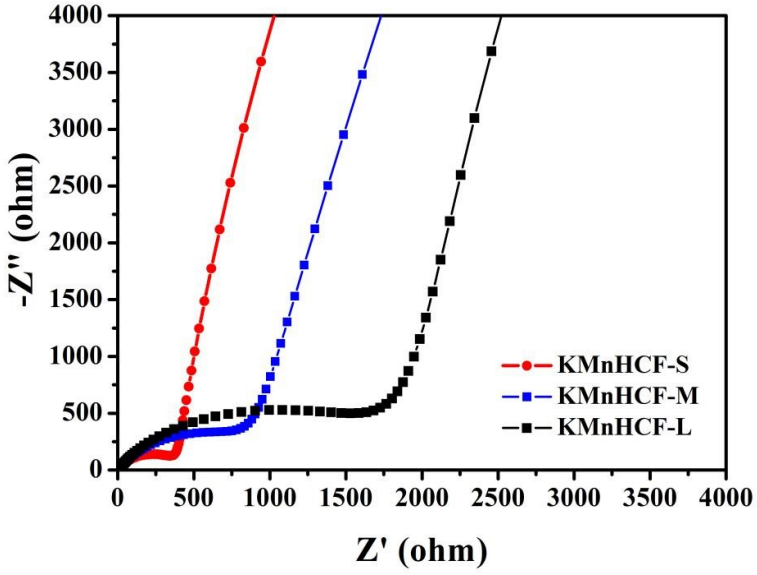

Fig. S12 Electrochemical impedance spectroscopy (EIS) of three samples after 200 cycles at 0.05 A g^{-1}.

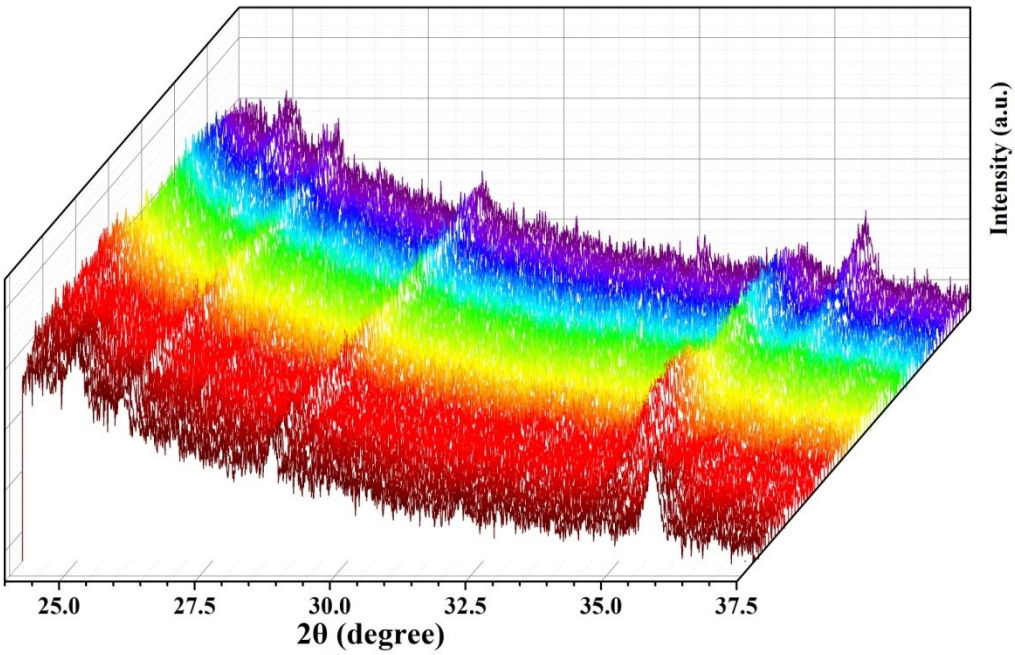

Fig. Sx In situ XRD patterns for KMnHCF-M.

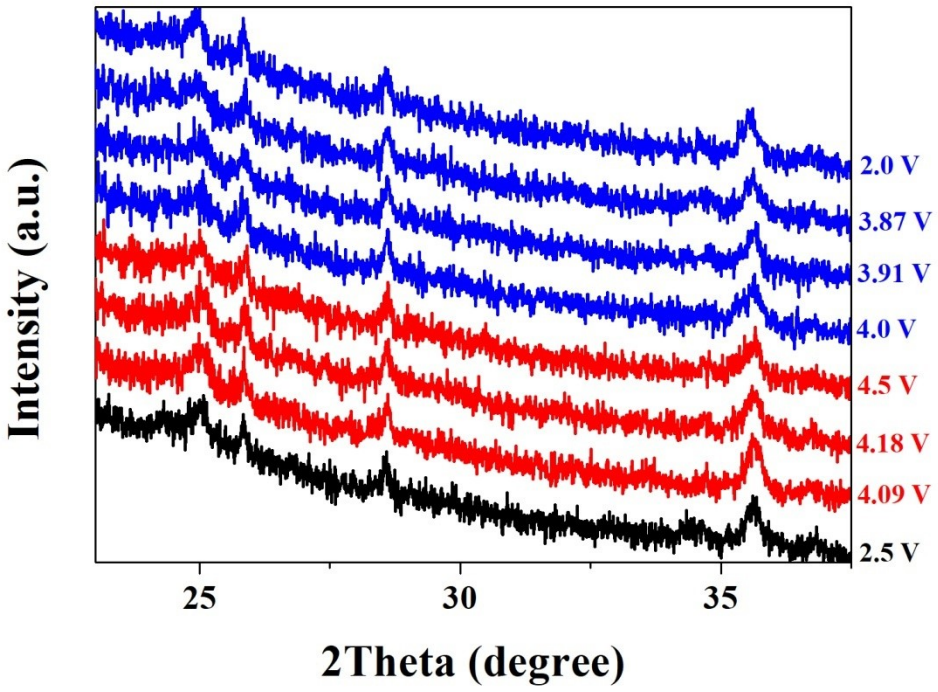

Fig. Sx The individual XRD results for KMnHCF-S under various state-of-charge.

Table S7. Mn-N bond length changes during phases transition.

	Mn-N bond length						
	N1	N2	N3	N4	N5	N6	Average
$K_2MnFe(CN)_6$	1.963	1.963	1.966	1.966	1.944	1.944	1.96
$KMnFe(CN)_6$	1.892	1.892	1.892	1.892	1.892	1.892	1.89
$MnFe(CN)_6$	1.871	1.871	1.794	1.794	1.794	1.794	1.82

Table S8. Mn-N bond length changes during the solid-solution reaction.

	Mn-N bond length						
	N1	N2	N3	N4	N5	N6	Average
$K_2MnFe(CN)_6$	1.963	1.963	1.966	1.966	1.944	1.944	1.96
$KMnFe(CN)_6$	1.916	1.916	1.939	1.939	1.901	1.901	1.92
$MnFe(CN)_6$	1.889	1.889	1.899	1.899	1.899	1.899	1.90

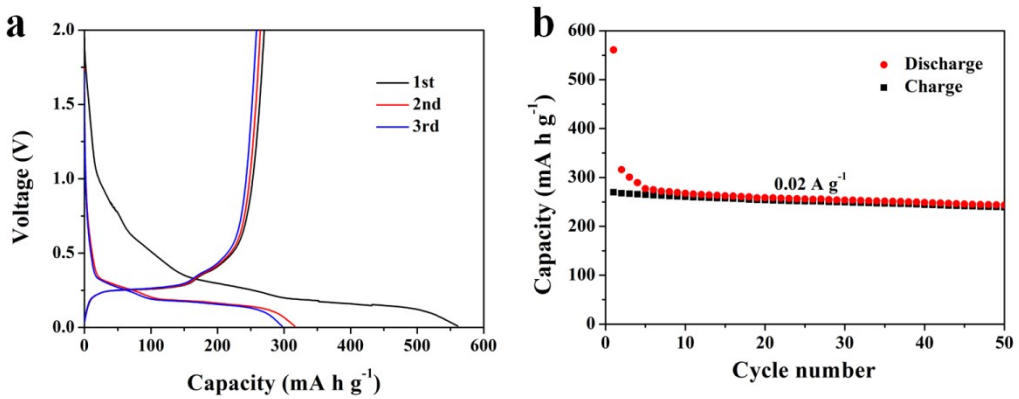

Fig. S13 (a) Discharging/charging curves and (b) cycling performance of graphite at 0.02 A g^{-1}.

Reference

1. G. Kresse and J. Hafner, *Phys. Rev. B*, 1993, **47**, 558-561.
2. G. Kresse and J. Furthmüller, *Phys. Rev. B*, 1996, **54**, 11169-11186.
3. G. Kresse and J. Furthmüller, *Comp. Mater. Sci.*, 1996, **6**, 15-50.
4. J. P. Perdew and Y. Wang, *Phys. Rev. B*, 1992, **45**, 13244-13249.
5. J. P. Perdew, K. Burke and M. Ernzerhof, *Phys. Rev. Lett.*, 1996, **77**, 3865-3868.
6. P. E. Blöchl, *Phys. Rev. B*, 1994, **50**, 17953-17979.
7. G. Kresse and D. Joubert, *Phys. Rev. B*, 1999, **59**, 1758-1775.
8. K. Momma and F. Izumi, *J. Appli. Crystallogr.*, 2011, **44**, 1272-1276.
9. L. Deng, J. Qu, X. Niu, J. Liu, J. Zhang, Y. Hong, M. Feng, J. Wang, M. Hu, L. Zeng, Q. Zhang, L. Guo and Y. Zhu, *Nat. Commun.*, 2021, **12**, 2167.